Nanoscale

Accepted Manuscript

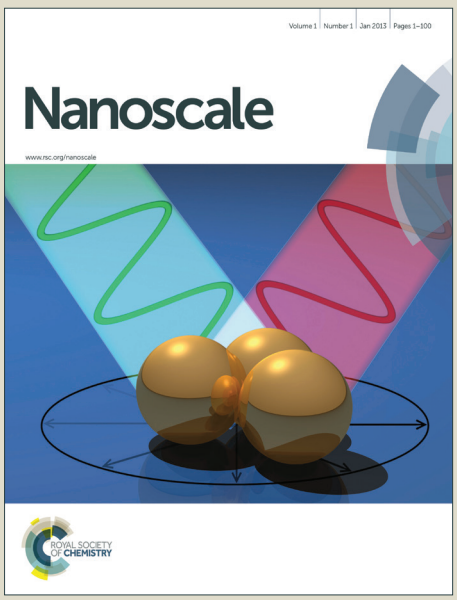

ROYAL SOCIETY OF CHEMISTRY

www.rsc.org/nanoscale

Unique Synthesis of Hollow Co_3O_4 Nanoparticles embedded in Thin Al_2O_3 Nanosheets for the Enhanced Lithium Storage

Jiao Yang, Hua-Jun Qiu, Liang Peng, Wenxiang Li, Yu Wang*

The State Key Laboratory of Mechanical Transmissions and School of Chemistry and Chemical Engineering, Chongqing University, Chongqing 400044, China

*Email: wangy@cqu.edu.cn; prospectwy@gmail.com

Abstract

The designed synthesis of advanced nanocomposite architecture is significant for their applications in energy storage, catalysis, sensing, etc. Herein, thin Al_2O_3 hexagon nanosheets with encapsulated hollow Co_3O_4 nanoparticles (Co_3O_4-HNPs) are successfully synthesized by using $Co_6Al_2CO_3(OH)_{16}{\cdot}4H_2O$ nanosheets as templates and followed by two step annealing process. When used as an anode material in lithium ion batteries (LIBs), the homogeneous Co_3O_4-HNPs/Al_2O_3 nanosheet composite exhibits an excellent performance with a high reversible capacity, rate capability, and enhanced cycling stability.

Keywords: hexagon nanosheet, encapsulated composite, hollow Co_3O_4, lithium ion batteries

Introduction

Developing advanced and green energy sources is very important for the sustainable development of modern society, especially with the decreasing amount of fossil energy sources and all these environmental problems caused by consuming them.[1, 2] As a green power source, lithium ion batteries (LIBs) have been widely used nowadays and also attracted great research interest to enhance their performance due to the importance.[3-6] At present, various materials such as nanostructured carbon,

transition metal oxides, transition metal phosphides, etc., have been prepared and studied as the anode materials for LIBs.[7-9] Among them, the transition metal oxides such as Co_3O_4 have attracted increasing research interest owing to its high theoretical capacity (890 mAh g^{-1}).[10-15] However, the remarkable volume changes and severe particle aggregation during the Li insertion/extraction reaction would lead to electrode pulverization, resulting in a significant capacity loss and poor cycling stability.[16, 17] To conquer these problems, various strategies have been utilized, including the synthesis of carbon-based nanocomposites, 1-D Co_3O_4 nanowires or 2-D Co_3O_4 nanosheets, hollow structure, etc.[10, 16, 18-21] Among these, the fabrication of composites with graphene and/or other metal oxides has been demonstrated to be quite successful.[22-24] However, these Co_3O_4-based composites are usually prepared by simply growing one component on the surface of the other.[10, 25-28] Due to the one-side simple attachment, the prepared composite structure may be easily damaged during continuous charge/discharge reactions. The encapsulation of one active component inside two closely attached thin nanosheets could be an effective strategy to enhance the structure integrity and stability.[29, 30] In our previous work, we have successfully designed and synthesized metal oxides nanoparticles (NPs) encapsulated in carbon nanosheets or nanotubes for enhanced Li storage.[10, 31] Besides, the coating of Al_2O_3 thin film on active materials has also been demonstrated to be a good strategy to enhance the structure stability of the active component in LiBs. For example, Cho et al., used a sol-gel method to coat Al_2O_3 on $LiCoO_2$ particle surface.[32] Kang et al., used an atomic layer deposition method to coat Al_2O_3 on Fe_3O_4 nanocrystal surface.[33] However, the facile synthesis of closely encapsulated Co_3O_4-HNPs inside of Al_2O_3 thin nanosheets remains a big challenge.

In this work, using $Co_6Al_2CO_3(OH)_{16}{\cdot}4H_2O$ hexagon nanosheets as templates, we successfully designed and fabricated uniform thin Al_2O_3 nanosheets with Co_3O_4-HNPs encapsulated inside and remain the precursor hexagon architecture. Due to the advanced structure design and enhanced material properties, the encapsulated hollow Co_3O_4-HNPs/Al_2O_3 nanosheets composite exhibits a large reversible capacity, excellent cycling stability and high rate capability when used as an anode material for LIBs.

Experimental Section

Synthesis of $Co_6Al_2CO_3(OH)_{16}{\cdot}4H_2O$ hexagon nanosheets.

Ammonia (12.5 mL), ethylene glycol (12.5 mL), $Co(NO_3)_2$ aqueous solution (5 mL, 1 M), $Al(NO_3)_3$ (2 mL, 1 M), and Na_2CO_3 solution (5 mL, 1 M) were added step-by-step into a baker under continuous stirring condition. After stirring for 20 min, the mixed solution changed into burgundy. After that, the precursor solution was transferred into a 50 mL Teflon-lined autoclave, sealed and heated at 180 °C for 15 h. After it was cooled to room temperature, the samples were taken out and washed by centrifugation with deionized water and pure ethanol. Finally, the samples were dried in an oven at 60 °C overnight.

Synthesis of Co_3O_4-HNPs /Al_2O_3 nanosheets.

The pink precursor was annealed at 750 °C for 200 min in a mixed H_2 and Ar atmosphere. After cooled to room temperature, the samples were further annealed at 450 °C for 200 min in air with a temperature programming of 1 °C /min. Because the composites is synthesis through annealing the precursor of $Co_6Al_2CO_3(OH)_{16}.4H_2O$ hexagon nanosheets. The molar ratio of Co and Al is 3:1 and the mass ratio of Co_3O_4 and Al_2O_3 is approximate 4.72:1. This indicates that the weight fraction of Co_3O_4 is 82.52% and can't be adjusted.

For comparison, pure Co_3O_4 NPs were prepared by mixing water (12.5 mL), ammonia (12.5 mL), $Co(NO_3)_2$ aqueous solution (5 mL, 1 M) under stirring. After stirring for 30 min, the mixture was transferred into a 50 mL Teflon-lined autoclave, sealed and heated at 170 °C for 24 h. After it was cooled to room temperature, the samples were taken out and washed with water and ethanol. Finally, the black samples were dried in an oven at 60 °C overnight.

Material Characterizations.

All the samples were characterized by a powder X-ray diffraction (Bruker D8 Advance X-ray diffractometer) with Cu Kα radiation, scanning electron microscope (SEM, JEOL, JSM-7800F) with an energy dispersive spectrometer (EDS), transmission electron microscopy (TEM, JEOL, JEM-2100F), and Brunauer-Emmett-Teller surface-area and pore-size analyzer (BET, Quantachrome Autosorb-6B).

Electrochemical Measurements

A lithium metal was used as the counter electrode and a Cellgard2400 membrane was used as the cell separator. The electrolyte was 1 M $LiPF_6$ in ethylene carbonate and diethyl carbonate (EC-DEC, v/v=1:1). The working electrode was prepared by a slurry coating method. The slurry was prepared by mixing 80 wt% Co_3O_4-HNPs/Al_2O_3 composite, 10 wt% carbon black and 10 wt% polyvinylidene fluoride (PVDF) dissolved in N-methyl-pyrrolidinone (NMP). A homogeneous mixture was formed by magnetic stirring for 24 h. This slurry was spread on copper foil with diameter of 12mm and dried at 80 ℃ for 24 h. The mass loading of the active material in the examined electrodes is about 2.2 mg cm^{-2}.The cells were constructed in an Ar-filled glove box under 20 MPa pressure. The galvanostatic cycling was performed on NEWARE battery program-control testing system at rate of 0.1-5 A g^{-1} with the voltage range of 0.01-3.0 V, and cyclic voltammetry (CV) was collected using Electrochemical workstation (CH660E) between 0 and 3 V with a scan rate of 0.2 mV/s. The specific capacity and current density were calculated based on the mass of the active material in the working electrode.

Results and discussion

Preparation and characterization of encapsulated Co_3O_4-HNPs/Al_2O_3 nanosheets

The fabrication procedure of the Co_3O_4-HNPs encapsulated in thin Al_2O_3 nanosheets is shown in Scheme 1a. First, pure $Co_6Al_2CO_3(OH)_{16}{\cdot}4H_2O$ hexagon nanosheets were synthesized by a hydrothermal method. The hexagon nanosheets were then annealed in H_2 and Ar atmosphere at 750 ℃. This annealing process would decompose (reduce) the cobalt element into metal Co NPs encapsulated inside of thin Al_2O_3 nanosheets which inherit the morphology of the precursor hexagon nanosheets. After that, a second annealing in air was carried out to transform the encapsulated Co NPs/Al_2O_3 nanosheets into hollow Co_3O_4-HNPs/Al_2O_3 nanosheets. As explained in previous work, the mechanism for the formation of Co_3O_4-HNPs from Co NPs is due to the nanoscale Kirkendall effect which has also been observed by annealing Ni or Cu NPs in different atmospheres.[34] For more electrode design strategies, one can refer to an excellent review published recently.[35]

Fig. 1a shows the SEM image of the synthesized $Co_6Al_2CO_3(OH)_{16}{\cdot}4H_2O$ nanosheets. It is observed that the thin nanosheets are relatively uniform with an

average size of around 300 nm and a thickness of ~20 nm. From the zoom-in SEM image (Fig. 1b), it is observed that the thin nanosheet precursor is hexagon. XRD analysis (Fig. 1c) shows that the formed nanosheets are pure $Co_6Al_2CO_3(OH)_{16}{\cdot}4H_2O$ (JCPDS No. 51-0045). After the first annealing in H_2 and Ar atmosphere, the morphology of the nanosheets is well-inherited by the formed Al_2O_3 nanosheets (Fig. 1d and 1e). The formed Co NPs with a size of ~8 nm are uniformly distributed inside of the thin Al_2O_3 nanosheets from the bright-field STEM image (Fig. 1e). The XRD pattern (Fig. 1f) shows three main peaks which can be assigned to the (111), (200) and (220) diffraction of face-centered cubic cobalt (JCPDS No. 89-7093). After the second step annealing, the structure of the encapsulated Co NPs/Al_2O_3 composite is well retained by the encapsulated Co_3O_4-HNPs/Al_2O_3 nanosheets (Fig. 2a and 2b). The composite is further characterized by TEM. As shown in Fig. 2c, high density and uniform Co_3O_4-HNPs with a diameter of ~15 nm are homogeneously encapsulated inside the thin Al_2O_3 nanosheets, which is in good agreement with the SEM result. The clear color contrast between the hollow core and surface shell indicates that the Co_3O_4-HNPs have a hollow structure. The continuous lattice fringes in the HRTEM image (Fig. 2d) indicate the crystalline nature of the encapsulated Co_3O_4-HNPs. The lattice spacing of 0.28 nm and 0.23 nm corresponds to the (220) and (222) plane of Co_3O_4, respectively. The crystal structure of the Co_3O_4-HNPs/Al_2O_3 nanosheets is further examined by XRD (Fig. 2e). The diffraction peaks at the degree of 31.2^o (220), 36.9^o (311), 55.7^o (422), 59.2^o (511) and 65.2^o (440) are consistent with the standard XRD data for Co_3O_4 (JCPDS No. 43-1003). The week peak at ~46^o can be ascribed to (400) diffraction of α-Al_2O_3. To further demonstrate the existence of α-Al_2O_3, we dissolved the Co_3O_4-HNPs in a weak HCl aqueous solution. After the dissolution, the porous α-Al_2O_3 is well preserved with inner holes (Fig. S1a and S1b in supporting information). XRD analysis further confirms the α-Al_2O_3 crystal structure (Fig. S1c). The Brunauer–Emmett–Teller (BET) surface area of the composite is determined to be ~208 $m^2\ g^{-1}$ and pore diameter is around 4 nm with the Barrett-Joyner-Hallender (BJH) method (Fig. 2f). These results suggest that the encapsulated Co_3O_4-HNPs/Al_2O_3 composites possess a high surface area and many small pores which would facilitate the free diffusion of electrolyte during electrochemical reactions.

The encapsulated Co_3O_4-HNPs in Al_2O_3 thin nanosheets are further characterized by EDS mapping. As shown in Fig. 3, the nano-composite is clearly comprised of Co, Al, and O. From the Fig. 3a and Fig. 3b, we can confirm that the encapsulated hollow NPs are Co oxides because the distribution of Co element is in good agreement with the hollow particles (two hollow particles are denoted by red circles).

Electrochemical measurement

The Al_2O_3 nanosheets with encapsulated Co_3O_4-HNPs were then tried as an anode material for LIBs. For comparison, we also synthesized pure Co_3O_4 NPs, which were characterized by SEM, TEM and XRD (Fig. S2). The diameter of the Co_3O_4 NPs is around 10 nm (Fig. S2a, S2b). The XRD pattern (Fig. S2c) confirms that the samples are pure Co_3O_4 (JCPDS No. 01-1152). Fig. 4a shows the galvanostatic discharge-charge curves of the Co_3O_4-HNPs/Al_2O_3 nanosheets at 0.1 A g^{-1} between 0.01 and 3.0 V (versus Li/Li^+). As shown that that the Co_3O_4-HNPs/Al_2O_3 nanosheets exhibit a high first discharge capacity of ~1787 mAh g^{-1}, which is much higher than the theoretical capacity of Co_3O_4 (890 mAh g^{-1}). The excess capacity discharged at first could be related to the initial formation of the solid-electrolyte-interface (SEI) layer caused by electrolyte degradation. It should be mentioned that the excess capacity during the first discharge is a common phenomenon and also detected in other anode materials.[36, 37] Compared to pure Co_3O_4 nanoparticles electrode (Fig. S4a), the plateau with slight lean in first discharge for the Co_3O_4-HNPs/Al_2O_3 nanocomposite may be due to the presence of Al_2O_3 nanosheets. It is possible that the Al_2O_3 nanosheets can adsorb and release Li during the Lithiation/delithiation, which may slightly affect the electrochemical behavior of Co_3O_4.[33, 38] The corresponding CV curves are shown in Fig. S3 which exhibits a typical electrochemical behavior of Co_3O_4 in LIB tests with oxidation peaks at ~2.2 V and reduction peaks at ~0.8 V. Started from the second cycle, the capacity decreases slightly to ~1278 mAh g^{-1} and the charge/discharge reactions become quite stable (Fig. 4a). As shown in Fig. 4b, after even 150 cycles at 0.1 A g^{-1}, the capacity is still over 95% with a very high Coulombic efficiency (~99%). In comparison, the capacity of the bare Co_3O_4 NPs decreases quickly with the increasing cycle number at the same current density (Fig. S4a). These results indicate the excellent cycling stability achieved by encapsulating Co_3O_4-HNPs in thin Al_2O_3 nanosheets. The stabilized specific capacity (~1215 mAh g^{-1} at 0.1 A g^{-1}) is

also very high when compared with many reported values from Co_3O_4-based anode materials such as Co_3O_4 octahedral nanocages (887 mAh g^{-1} at 0.2 C), Co_3O_4/graphene composite (754 mAh g^{-1} at 0.1 A g^{-1}) and Co_3O_4/carbon nanotubes (823 mAh g^{-1} at 0.2 A g^{-1}).[24, 39, 40] A detailed comparison is shown in Tabel S1. To test the rate capability of the Co_3O_4-HNPs/Al_2O_3 nanocomposite, we sequentially increased the current density from 0.1 A g^{-1} to 5 A g^{-1}. As shown in Fig. 4c, the capacity decreases with the increasing current densities. When 5 A g^{-1} is applied, the capacity is still ~643 mAh g^{-1} (~53%), which also higher than those of previous reports,[39, 41] indicating the good rate capability of the encapsulated Co_3O_4-based composite electrode. Moreover, when cycled back to 0.1 A g^{-1}, the recovered capacity can reach ~1152 mAh g^{-1}, which further demonstrates the excellent performance of the designed composite electrode (Fig. 4d). To evaluate the contribution from the Al_2O_3, we also use the bare Al_2O_3 (Co_3O_4 has been dissolved in an acidic solution) as anode material in LIBs. The obtained result is similar to the result reported before.[42] Based on the charge/discharge curve of bare Al_2O_3 (Fig. S4b), we can see that the specific capacity is ~80 mAh g^{-1} at 0.1 A g^{-1}. It is concluded that the contribution from Al_2O_3 is very low and the overall capacity mainly comes from the active material Co_3O_4.

We also tested the ion and electronic resistance of the Co_3O_4-HNPs/Al_2O_3 nanocomposite and bare Co_3O_4 NPs, respectively (Fig. S5). The as-prepared Co_3O_4-HNPs/Al_2O_3 nanocomposite has a similar semicircle compared with bare Co_3O_4 NPs. This suggests that the Al_2O_3 thin film does not have any negative effect on the conductivity of the electrode. Thus, the high rate performance of Co_3O_4-HNPs/Al_2O_3 nanocomposite should be ascribed to the short Li^+ ion diffusion length and low internal charge-transfer resistance of the electrode.[43, 44] The SEM image of Co_3O_4-HNPs/Al_2O_3 after charge/discharge cycles can be seen in supporting information (Fig. S6). It is observed that most of the nanocomposites maintain the original architecture, which is consistent with the good electrochemical stability.

The high and stable charge/discharge performance should be owing to the designed advanced structure of the electrode. Firstly, the porous Al_2O_3 thin nanosheets can remarkably enhance the diffusion of electrolyte and ions.[25] Moreover, due to the encapsulation in the thin Al_2O_3 nanosheets, the detachment, aggregation, and even

pulverization of the Co_3O_4-HNPs can be largely solved. Secondly, the efficient inner space from the Co_3O_4-HNPs would allow the volume change of the Co_3O_4 nano-shells while retaining the structure integrity.[45, 46] Last but not least, the nanoscale Co_3O_4 hollow particles (~15 nm) with high surface areas will effectively improve the Li-ion exchange rate.

Conclusions

Uniform Al_2O_3 hexagon nanosheets with encapsulated hollow Co_3O_4-HNPs was facilely prepared by using $Co_6Al_2CO_3(OH)_{16}{\cdot}4H_2O$ nanosheets as templates, and followed by two-step annealing process. This designed and synthesized composite material possesses many advanced structure properties such as intimate contact between the encapsulated hollow Co_3O_4-HNPs and thin Al_2O_3 nanosheets, high nanoporosity, large specific surface area, etc. Owing to the unique nano-architecture, the Co_3O_4-HNPs/Al_2O_3 nanoheets exhibits a high and stable Li storage capability when used as an anode material in LIBs. The strategy presented in this work may be helpful for designing advanced encapsulated nanocomposites for various applications such as catalysis, sensing, etc.

Acknowledgements

This work was financially supported by the Thousand Young Talents Program of the Chinese Central Government (Grant No.0220002102003), National Natural Science Foundation of China (NSFC, Grant No. 21373280 , 21403019), Beijing National Laboratory for Molecular Sciences (BNLMS), the Fundamental Research Funds for the Central Universities (0301005202017) and Hundred Talents Program at Chongqing University (Grant No. 0903005203205).

Reference

1. J. Chmiola, C. Largeot, P. L. Taberna, P. Simon and Y. Gogotsi, *Science*, 2010, **328**, 480-483.
2. H. Sun, X. You, J. E. Deng, X. L. Chen, Z. B. Yang, J. Ren and H. S. Peng, *Adv. Mater.*, 2014, **26**, 2868-2873.
3. M. Armand and J. M. Tarascon, *Nature*, 2008, **451**, 652-657.
4. S. Y. Liu, J. Xie, Q. M. Su, G. H. Du, S. C. Zhang, G. S. Cao, T. J. Zhu and X. B. Zhao, *Nano Energy*, 2014, **8**, 84-94.
5. J. Liu, K. P. Song, P. A. van Aken, J. Maier and Y. Yu, *Nano Lett.*, 2014, **14**, 2597-2603.
6. C. J. Niu, J. S. Meng, C. H. Han, K. N. Zhao, M. Y. Yan and L. Q. Mai, *Nano Lett.*, 2014, **14**, 2873-2878.
7. M. S. Whittingham, *Chem. Rev.*, 2004, **104**, 4271-4301.
8. D. H. Wang, D. W. Choi, J. Li, Z. G. Yang, Z. M. Nie, R. Kou, D. H. Hu, C. M. Wang, L. V. Saraf, J. G. Zhang, I. A. Aksay and J. Liu, *ACS Nano*, 2009, **3**, 907-914.
9. J. S. Chen, H. Liu, S. Z. Qiao and X. W. Lou, *J. Mater. Chem.*, 2011, **21**, 5687-5692.
10. H.-J. Qiu, L. Liu, Y.-P. Mu, H.-J. Zhang and Y. Wang, *Nano Res.*, 2014, **8**, 321-339.
11. M. V. Reddy, G. V. Subba Rao and B. V. R. Chowdari, *Chem. Rev.*, 2013, **113**, 5364-5457.
12. C. Peng, B. Chen, Y. Qin, S. Yang, C. Li, Y. Zuo, S. Liu and J. Yang, *ACS Nano*, 2012, **6**, 1074-1081.
13. Y. Sun, X. Hu, W. Luo and Y. Huang, *J. Phys. Chem. C*, 2012, **116**, 20794-20799.
14. K. Xie, P. Wu, Y. Zhou, Y. Ye, H. Wang, Y. Tang, Y. Zhou and T. Lu, *ACS Appl. Mater. Interfaces*, 2014, **6**, 10602-10607.
15. C. Zhou, Y. Zhang, Y. Li and J. Liu, *Nano Lett.*, 2013, **13**, 2078-2085.
16. Z. S. Wu, W. C. Ren, L. Wen, L. B. Gao, J. P. Zhao, Z. P. Chen, G. M. Zhou, F. Li and H. M. Cheng, *ACS Nano*, 2010, **4**, 3187-3194.
17. H. Wu, M. Xu, Y. C. Wang and G. F. Zheng, *Nano Res.*, 2013, **6**, 167-173.
18. Y. Wang, H. J. Zhang, L. Lu, L. P. Stubbs, C. C. Wong and J. Y. Lin, *ACS Nano*, 2010, **4**, 4753-4761.
19. H. J. Liu, S. H. Bo, W. J. Cui, F. Li, C. X. Wang and Y. Y. Xia, *Electrochim. Acta*, 2008, **53**, 6497-6503.
20. W. Ni, J. Cheng, L. Shi, X. Li, B. Wang, Q. Guan, L. Huang, G. Gu and H. Li, *J. Mater. Chem. A*, 2014, **2**, 19122-19130.
21. X. Wang, X. L. Wu, Y. G. Guo, Y. T. Zhong, X. Q. Cao, Y. Ma and J. N. Yao, *Adv. Funct. Mater.*, 2010, **20**, 1680-1686.
22. J. Zhi, S. Deng, Y. Zhang, Y. Wang and A. Hu, *J. Mater. Chem. A*, 2013, **1**, 3171-3176.
23. F. Zhang, T. Zhang, X. Yang, L. Zhang, K. Leng, Y. Huang and Y. Chen, *Energy Environ. Sci.*, 2013, **6**, 1623-1632.
24. L. Zhuo, Y. Wu, J. Ming, L. Wang, Y. Yu, X. Zhang and F. Zhao, *J. Mater. Chem. A*, 2013, **1**, 1141-1147.
25. Y. Lu, X. Wang, Y. Mai, J. Xiang, H. Zhang, L. Li, C. Gu, J. Tu and S. X. Mao, *J. Phys. Chem. C*, 2012, **116**, 22217-22225.
26. G. Zhou, D.-W. Wang, F. Li, L. Zhang, N. Li, Z.-S. Wu, L. Wen, G. Q. Lu and H.-M. Cheng, *Chem. Mater.*, 2010, **22**, 5306-5313.

27. S. Yang, X. Feng, S. Ivanovici and K. Müllen, *Angew. Chem. Int. Edit.*, 2010, **49**, 8408-8411.
28. S.-W. Kim, D.-H. Seo, H. Gwon, J. Kim and K. Kang, *Adv. Mater.*, 2010, **22**, 5260-5264.
29. Y. Wang, Y. Bai, X. Li, Y. Feng and H. Zhang, *Chem. Eur. J.*, 2013, **19**, 3340-3347.
30. H. Zhang, Y. Bai, Y. Feng, X. Li and Y. Wang, *Nanoscale*, 2013, **5**, 2243-2248.
31. L. Peng, Y. Feng, Y. Bai, H.-J. Qiu and Y. Wang, *J. Mater. Chem. A*, 2015, **3**, 8825-8831.
32. J. Cho, Y. J. Kim and B. Park, *Chem. Mater.*, 2000, **12**, 3788-3791.
33. E. Kang, Y. S. Jung, A. S. Cavanagh, G.-H. Kim, S. M. George, A. C. Dillon, J. K. Kim and J. Lee, *Adv. Funct. Mater.*, 2011, **21**, 2430-2438.
34. J. G. Railsback, A. C. Johnston-Peck, J. W. Wang and J. B. Tracy, *ACS Nano*, 2010, **4**, 1913-1920.
35. Y. Tang, Y. Zhang, W. Li, B. Ma and X. Chen, *Chem. Soc. Rev.*, 2015, **44**, 5926-5940.
36. H. Zhong, G. Yang, H. Song, Q. Liao, H. Cui, P. Shen and C.-X. Wang, *J. Phys. Chem. C*, 2012, **116**, 9319-9326.
37. B. Wang, J. S. Chen, H. B. Wu, Z. Wang and X. W. Lou, *J. Am. Chem. Soc.*, 2011, **133**, 17146-17148.
38. M. Yu, A. Wang, Y. Wang, C. Lia and G. Shi, *Nanoscale*, 2014, **6**, 11419-11424.
39. D. Liu, X. Wang, W. Tian, Y. Bando and D. Golberg, *Sci. Rep.*, 2013, **3**, 2543-2548.
40. S. Yang, G. Cui, S. Pang, Q. Cao, U. Kolb, X. Feng, J. Maier and K. Mullen, *ChemSusChem*, 2010, **3**, 236-239.
41. A. Q. Pan, Y. P. Wang, W. Xu, Z. W. Nie, S. Q. Liang, Z. M. Nie, C. M. Wang, G. Z. Cao and J. G. Zhang, *J. Power Sources*, 2014, **255**, 125-129.
42. B.-C. Yu, J.-O. Lee, J. H. Song, C.-M. Park, C. K. Lee and H.-J. Sohn, *J. Solid State Electrochem.*, 2012, **16**, 2631-2638.
43. Y. Tang, Y. Zhang, J. Deng, D. Qi, W. R. Leow, J. Wei, S. Yin, Z. Dong, R. Yazami, Z. Chen and X. Chen, *Angew. Chem. Int. Ed.*, 2014, **53**, 13488-13492.
44. Y. Tang, Y. Zhang, J. Deng, J. Wei, H. Le Tam, B. K. Chandran, Z. Dong, Z. Chen and X. Chen, *Adv. Mater.*, 2014, **26**, 6111-6118.
45. L. Zhang, H. B. Wu, S. Madhavi, H. H. Hng and X. W. Lou, *J. Am. Chem. Soc.*, 2012, **134**, 17388-17391.
46. J. F. Li, J. Z. Wang, D. Wexler, D. Q. Shi, J. W. Liang, H. K. Liu, S. L. Xiong and Y. T. Qian, *J. Mater. Chem. A*, 2013, **1**, 15292-15299.

Figure captions:

Scheme 1. Schematic illustration of the designed synthesis process of the hollow Co_3O_4-HNPs/Al_2O_3 nanosheets composite.

Fig. 1. SEM/STEM images of $Co_6Al_2CO_3(OH)_{16}{\cdot}4H_2O$ nanosheets before (a, b) and after (d: STEM image, e) the first annealing. (a and d: low magnification; b and e: high magnification) and XRD patterns of the precursors before (c) and after (f) the first annealing process.

Fig. 2. SEM images (a, b), TEM (c), HRTEM (d), XRD pattern (e) and nitrogen absorption/desorption curve (f) of the Co_3O_4-HNPs/Al_2O_3 nanosheet composite. Inset in (f) is the corresponding pore size distribution.

Fig. 3. STEM image (a) and EDS mapping results (b, c and d) of the encapsulated Co_3O_4-HNPs/Al_2O_3 nanosheet composite.

Fig. 4. Galvanostatic charge-discharge curves at different cycles at 0.1 A g^{-1} (a). Cycling performance and coulombic efficiency at a current density of 0.1 A g^{-1} (b). Galvanostatic charge-discharge curves (c) at different current densities and the rate capability results (d) of the encapsulated hollow Co_3O_4-HNPs/Al_2O_3 nanosheet composite.

Scheme 1

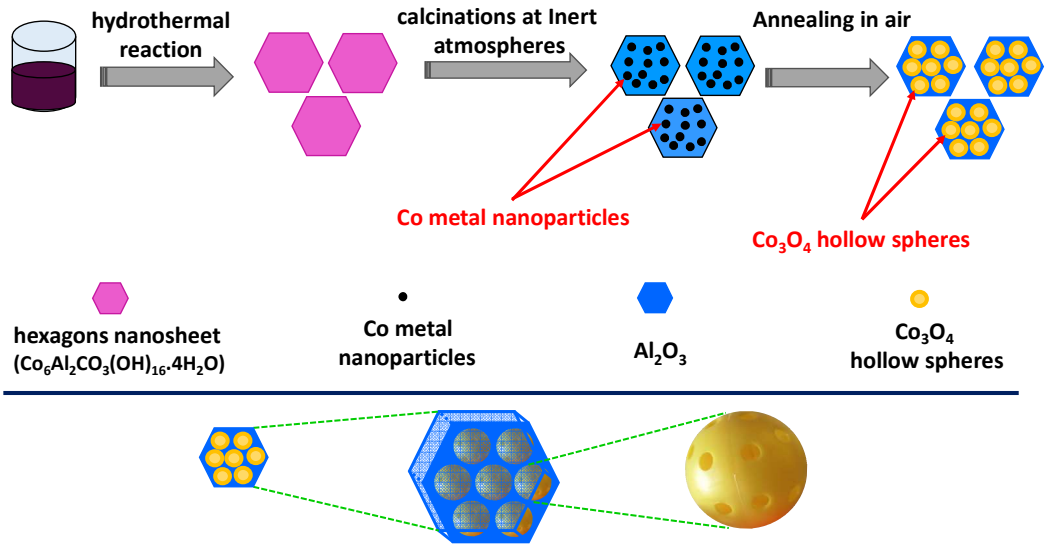

Fig. 1

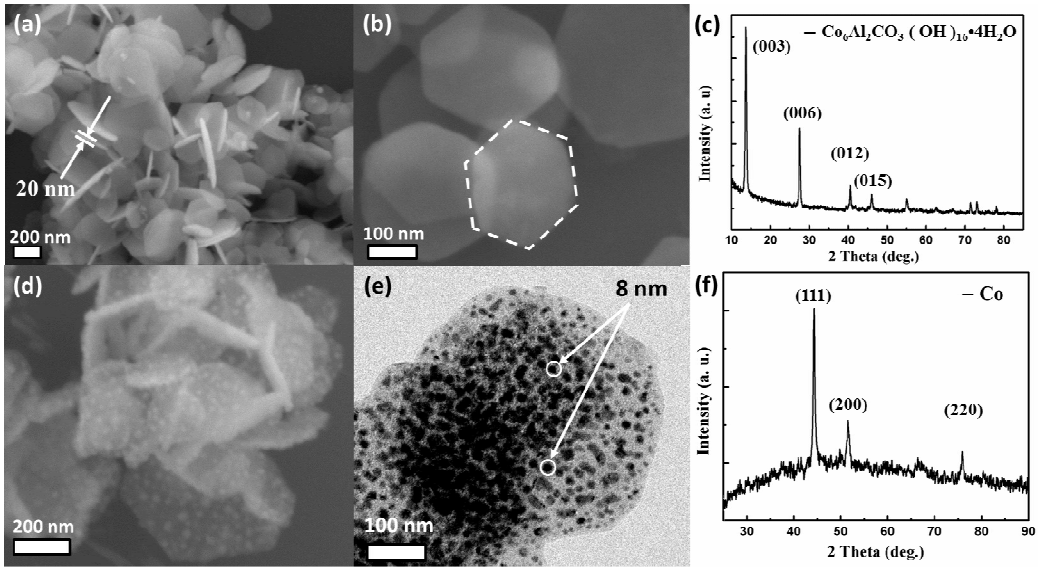

Fig. 2

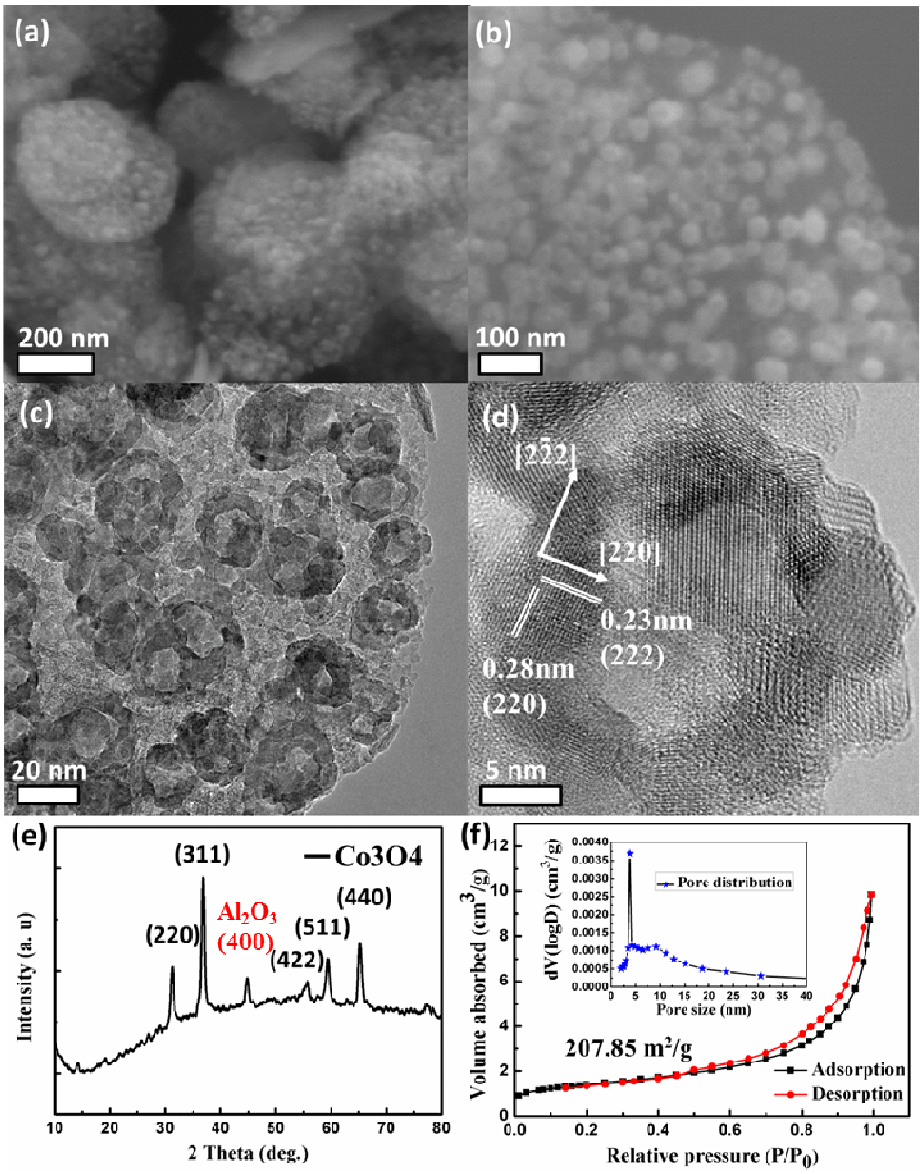

Fig. 3

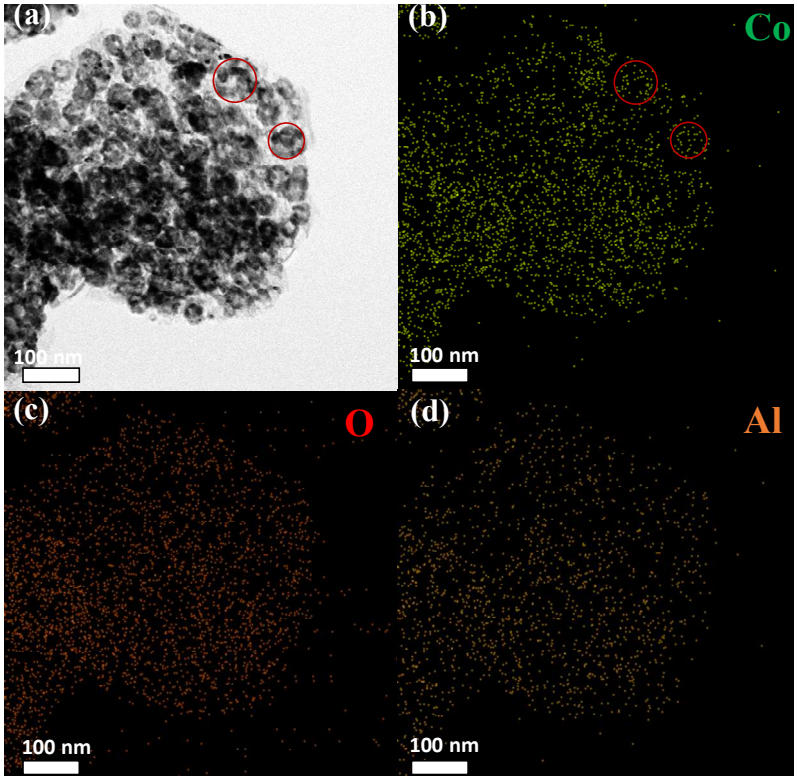

Fig. 4

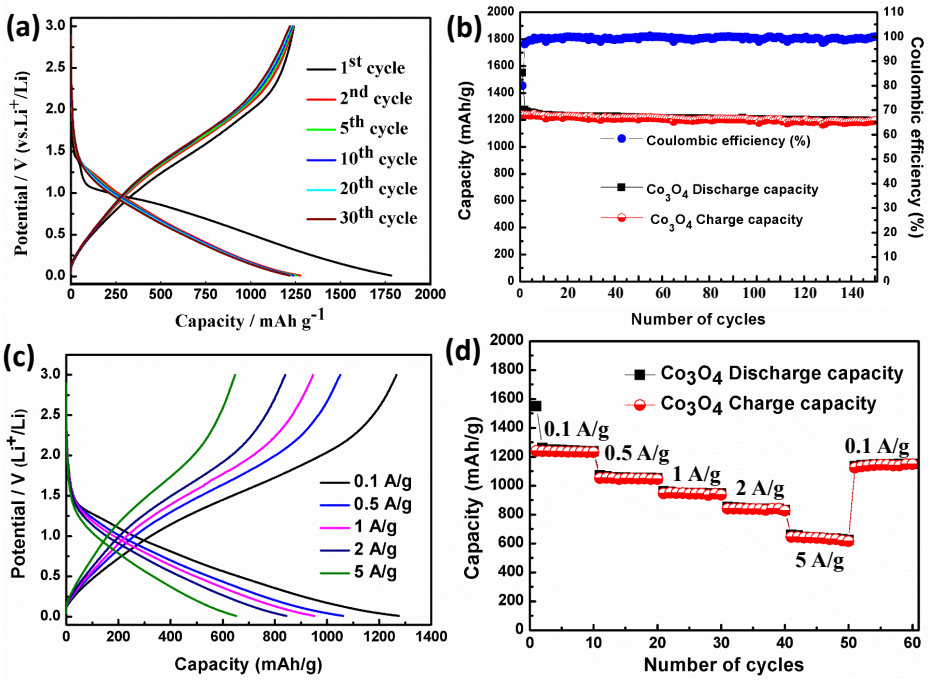

A table of contents:

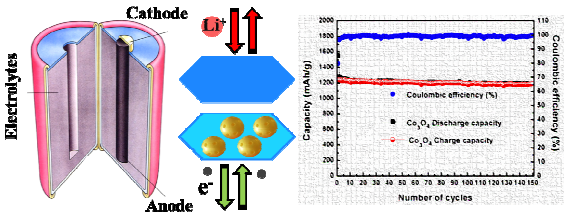

Hollow Co_3O_4 nanoparticles encapsulated in thin Al_2O_3 hexagon nanosheets are fabricated and exhibit an excellent performance in LIBs.